# Cage-to-cage migration rates of Xe atoms in zeolite NaA from magnetization transfer experiments and simulations

A. Keith Jameson
*Department of Chemistry, Loyola University, Chicago, Illinois 60626*

Cynthia J. Jameson and Rex E. Gerald II
*Department of Chemistry, University of Illinois at Chicago, 845 W. Taylor, Chicago, Illinois 60607*

(Received 19 January 1994; accepted 18 April 1994)

Xenon trapped in the alpha cages of zeolite NaA exhibits distinct NMR signals for clusters $Xe_1$, $Xe_2$, $Xe_3$,..., up to $Xe_8$. Using multisite magnetization transfer experiments, we have measured the rate constants $k_{mn}$ for the elementary processes that are involved in the cage-to-cage transfer of Xe atoms in the zeolite NaA, that is, for a single Xe atom leaving a cage containing $Xe_n$ to appear in a neighboring cage containing $Xe_{m-1}$, thereby forming $Xe_m$. In a random walk simulation, these rate constants reproduce over a hundred magnetization decay/recovery curves that we have measured in four samples of Xe in zeolite NaA at room temperature, in selective inversion, and complementary experiments for all the significantly populated clusters. The simulations also lead to the correct experimental equilibrium distributions, that is, the fractions of the alpha cages containing $Xe_1$,$Xe_2$,...,$Xe_8$.

## I. INTRODUCTION

Intracrystalline transport processes are important factors in the applications of zeolites to catalysis and selective sorption. Methods for studying diffusion of molecules sorbed in zeolites can be separated into two classes depending on the scale in which the translational motion of the molecule is followed:[1,2] In macroscopic methods such as uptake rate, frequency response, and flow methods, the length scale is the crystallite size. The measurements correspond to diffusion across a large number of unit cells. In microscopic methods such as pulsed field gradient NMR and neutron diffraction the length scale is a few tens of an Å, comparable to the dimensions of the cavities or channels. The macroscopic methods occur in nonequilibrium conditions (concentration gradients exist) which can provide the transport diffusivity whereas the microscopic methods tag the molecules and monitor the displacement of the tagged molecules among the untagged molecules under equilibrium conditions. This provides the self-diffusivity. These experimental methods involve complex molecular processes and discrepancies of up to two orders of magnitude in the derived diffusion coefficients that present problems to the theorists attempting to understand such diffusion processes at a molecular level via molecular dynamics simulations.

There have been estimates of microscopic rates. The model used is that in which the molecule performs instantaneous jumps separated by residence times in sites. For example, the width of the quasielastic neutron scattering of $CH_4$ in zeolite NaCaA provides a mean residence time of $4\times10^{-10}$ s.[3] In a similar spirit, the mean residence time of a $CH_4$ molecule in a cavity of zeolite NaA at room temperature is deduced to be 1.5 or $5\times10^{-8}$ s,[4] from the transverse relaxation time of the proton spins. However, these methods do not provide a direct experimental measure of rate constants, the connection with the measured quantity is an indirect one necessitating a specific interpretation of the observed quantity (which may not be independently verifiable) to provide an estimate.

A direct measurement of the rate constant for a well-defined molecular process, namely for a molecule leaving one cage and appearing in a neighboring cage, would be very useful. We present in this paper the elementary rate constants $k_{mn}$ for the cage-to-cage migration of a Xe atom in zeolite NaA, that is, for a single Xe atom leaving a cage containing $Xe_n$ to appear in a neighboring cage containing $Xe_{m-1}$, thereby forming $Xe_m$.

In previous papers we have demonstrated that the $^{129}Xe$ NMR chemical shifts of the xenon trapped in the alpha cages of zeolite NaA are sufficiently large to reveal the individual numbers of xenon atoms trapped in the alpha cages of the zeolite.[5] The intensities of the peaks for $Xe_1$,$Xe_2$,$Xe_3$,...,$Xe_8$ lead to the fractions $f(n)$ of the alpha cages containing 0,1,2,3,...,8 Xe atoms. If the adsorbed xenon is at equilibrium with the gas phase under the conditions of the experiment, then these give the equilibrium distribution at that temperature. We have been able to reproduce these equilibrium distributions in ten samples of Xe in NaA from low loading (0.45 Xe atoms per cage) to high loading (6.73 Xe atoms per cage) at 296 and 360 K by grand canonical Monte Carlo (GCMC) simulations.[6] The same GCMC simulations reproduce the average $^{129}Xe$ NMR chemical shifts of each cluster, including the large incremental shift in going from $Xe_6$ to $Xe_7$ and between $Xe_7$ and $Xe_8$. The temperature dependence of these chemical shifts is also reproduced. The GCMC simulations provide a good accounting of the equilibrium properties of the system, including the adsorption isotherm which had been measured in the NMR spectrum of the same samples. Although the peaks in the NMR spectrum are distinct, the system is in dynamic equilibrium: cage-to-cage migration is taking place at a rate that is too slow to collapse the peaks. In order to monitor this cage-to-cage migration we propose to tag a particular set of Xe atoms, only the $Xe_6$ for example. As seen in Fig. 1, when a single Xe atom leaves the

 0021-9606/94/101(3)/1775/12/$6.00  

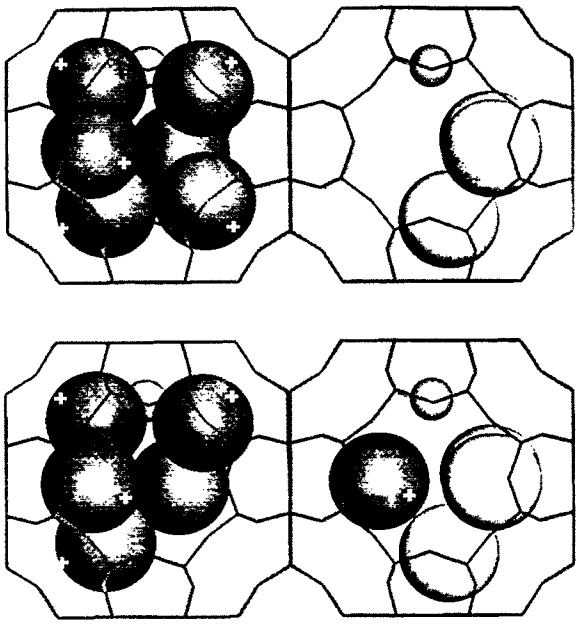

FIG. 1. A schematic representation of a jump event in which one Xe atom leaves the $Xe_6$ cluster and jumps into a neighboring cage containing the $Xe_3$ cluster. The elementary rate constant for this process is called $k_{46}$. When, as shown, the atoms in the $Xe_6$ cluster are labeled at time zero, the label can be tracked as it appears in the other clusters such as $Xe_5$ and $Xe_4$. $Na^+$ ions in the lattice are depicted by + signs except for the unique one which is shown as a small sphere.

cage containing the tagged cluster to jump into a neighboring cage (in this example) containing a $Xe_3$ cluster, the tag disappears from the $Xe_6$, and appears in the $Xe_4$ and the remaining $Xe_5$. Since it is the number of Xe atoms that are trapped together that determines its resonance frequency in the spectrum, the tag can be followed as the tagged atoms become part of various $Xe_n$ clusters. The simplicity of the system allows us to attach a detailed microscopic picture to the individual microscopic rate constants that are associated with the elementary steps of cage-to-cage migration such as the one illustrated in Fig. 1. The use of related NMR techniques to study the rates of cage-to-cage migration of Xe atoms in NaA were ongoing concurrently in two laboratories: Pines in Berkeley and ours. Both groups reported their results in the same symposium in March 1993.[7,8] The Pines results have been published, and we cite explicitly in this paper the specific areas of overlap.

## II. METHODS

The study of chemical exchange by monitoring the transfer of polarization can be carried out by many techniques. Pines *et al.* have used two-dimensional exchange spectroscopy to study this system.[8] Another possibility is a one-dimensional experiment in which one selectively inverts the magnetization at site $A$ and monitors the recovery both of this resonance and that of sites $B$, $C$, etc., with which it is exchanging. The use of the DANTE (delays alternating with nutations for tailored excitation) sequences for selective inversion[9] has the advantage that total flip angle and selectivity may be controlled independently, without changing the pulse power. Because the individual peaks are well resolved, it is possible to selectively excite one cluster at a time. Several methods of analysis of the data for multisite exchange are in current use.[10,11] It has been shown that the magnetizations $M$ in a selective inversion recovery experiment on a chemically exchanging system follow the modified Bloch equations, conveniently written in matrix form

$$d\mathbf{M}/dt = \mathbf{KM} + \mathbf{M}^e, \tag{1}$$

where $M_i(t)$ is the $z$ magnetization of the $i$th site at time $t$, $M_i^e = M_i(\infty)/T_{1i}$, $M_i(\infty)$ is the equilibrium magnetization at the $i$th site, and $T_{1i}$ is the spin lattice relaxation time for magnetization at site $i$. The $n \times n$ matrix $\mathbf{K}$ has elements $K_{ji}$ for $i \neq j$ while the diagonal elements are given by

$$K_{ii} = -1/T_{1i} - \Sigma_{i \neq j} K_{ji}. \tag{2}$$

The phenomenological rate constant $K_{ji}$ describes the pseudo-first-order exchange rate from site $i$ to site $j$. The particular system of Xe clusters trapped in zeolite NaA alpha cages is simpler than others in which multisite magnetization transfer experiments have been applied in that there are no cross relaxations between clusters other than chemical exchange. On the other hand this system is more complex than other multisite magnetization transfer experiments in that the interpretation of the phenomenological rate constants in terms of microscopic elementary rate constants is not trivial, that is, the larger phenomenological rate constants are a composite of several microscopic rate constants. The microscopic rate constants are the interesting quantities, of course, the rate constants associated with the transfer of one Xe atom from one cage into a neighboring cage. The complementary experiment in which the other signals are selectively inverted provides another set of independent combinations of the unknown phenomenological rate constants. The advantage of these magnetization transfer experiments is that each experiment covers the maximum possible temporal and dynamical ranges since $M(t)$ can vary from $-M(\infty)$ to $+M(\infty)$, consequently a maximum of experimental information about the rate constants can be obtained. It has been demonstrated[10,12] that the signal recovery curves from the $n$ selective inversion experiments and the $n$ complementary experiments can be analyzed simultaneously to determine the $n(n-1)/2$ possible exchange rates in a general $n$-site case. The $n$ different relaxation rates will be measured independently by separate experiments, although in principle, all rates (including the relaxation times) could be determined from the $n \times n$ curves since there will be a surplus of information.

The simulations of the magnetization decay/recovery curves are carried out in a Monte Carlo scheme. Five thousand alpha cages represent the system. Suppose we are given a set of elementary rate constants; we use the notation that $k_{mn}$ is associated with the rate of transfer of a single Xe atom from a cage containing the cluster $Xe_n$ into a neighboring cage containing the cluster $Xe_{m-1}$ thereby making the new cluster $Xe_m$. This is consistent with the notation of Led for the phenomenological rate constants.[12] We assume that the jumps are uncorrelated; that is, a Xe atom attempting a jump out of a cage does not need to know whether another Xe is

attempting a jump at the same time. A time step is chosen ($\tau$) such that none of the probabilities $P_{mn}=\tau k_{mn}$ or $\tau/T_1$ exceed 0.50. The experimental relaxation times are used for the simulations in this paper. During this fixed time increment $\tau$, the transfers out of each of 5000 cages are carried out according to the following algorithm:

(1) Each Xe atom in the cage $i$ is allowed one attempt to leave.

(2) If the atom carries a beta spin, relaxation is contemplated by comparing a random number $r_1$ picked from a uniform distribution between 0.0 and 1.0, with the spin conversion probability $\tau/T_1$.

(3) A jump is contemplated; a recipient cage $j$ is chosen randomly from the other 4999 cages. If $j$ is full (contains $Xe_8$) the attempt to jump into it fails. If not full, the random number $r_2$ is compared with the probability of the event ($\tau k_{mn}$) where $m$ is one more than the number of Xe atoms in the recipient cage (that is, the new cluster to be formed is $Xe_m$).

(4) Go on to the next atom in the cage $i$.

(5) The process goes on in all 5000 cages in sequential order.

(6) This constitutes one time step.

Each simulated Dante or complementary magnetization transfer experiment is set up as follows. (a) The appropriate number of Xe atoms (according to the $\langle n\rangle$ of the sample) are distributed uniformly into the 5000 cages. (b) The approach to thermal equilibrium distribution is simulated by jumps as outlined above, except that spins are not assigned and relaxation is not considered. This is typically done in 2000 time steps. The thermal equilibrium distribution reached is the starting point for the simulation of the magnetization experiment. (c) Beginning with the thermal equilibrium distribution of particles among the 5000 cages, the initial conditions (magnetization in each cage at time zero) are set according to the experimental efficiency of the actual Dante or complementary experiment. That is, a known % of the alpha spins in cages containing $Xe_n$ are converted into beta spins to prepare the zero-time conditions. (d) The transfers between cages are carried out as described above for a total number of time steps equal to a duration of 3 s. After each time step, the total magnetizations of $Xe_1, Xe_2, ..., Xe_8$ are stored. The magnetization decay/recovery curves are obtained by signal averaging over 25 repetitions, that is, (c) and (d) are repeated to accumulate 25 scans of the Dante experiment (or complementary experiment).

The simulation of the equilibrium distributions in all the samples is carried out using the same $k$ matrix. The part of the algorithm dealing with the approach to thermal equilibrium is carried out for 1000 time steps and $f(n)$ data are accumulated over another 1000 time steps, to find the equilibrium $f(n)$ to which the set of rate constants lead in the ten samples with $\langle n\rangle$ ranging from 0.45 to 6.73. The simulation of the self-diffusion is carried out using the same $k$ matrix in a simulation box of $10\times10\times10$ cages using periodic boundary conditions.

## III. EXPERIMENT

Samples contain accurately known amounts of xenon and NaA in a known sample volume. The tube volume is approximately 0.25 mL containing about 40–50 mg of zeolite. The zeolite is dried (under thin-bed conditions) at 300–350 °C for at least 16 h. After preparation the sample is ramped down in temperature in a regulated oven from 300 to 80 °C in about 5 days. After a subsequent two weeks the sample becomes equilibrated at room temperature. In this manner, equilibrium distributions of Xe in the zeolite cages are reached much faster than the 3 months required without temperature programming. Enriched $^{129}Xe$ (>99%, ICON, Mount Marion, NY) was used.

At equilibrium our samples frequently have significant amounts of Xe both adsorbed and in the gas. A mass balance can be carried out by using the chemical shift of the gas to deduce its density, the number of moles in the gas is calculated by knowing the free volume occupied by the gas, and this is subtracted from the known number of moles of xenon introduced into the sample to obtain the number of Xe atoms contained in the known number of zeolite cages. This gives $\langle n\rangle$, the average number of Xe atoms per cage.

The magnetization transfer experiments were carried out in the available 10 mm probe on a Bruker AM-400, 9.4 T high resolution FT NMR spectrometer. Another set of experiments were carried out on a Varian VXR-300S, 7 T spectrometer. Selective inversion of a single peak was performed using a modification of the traditional DANTE experiment.[9] A series of sixteen $\pi/16$ pulses produce the selective $\pi$ pulse, with a cyclical 90° phase shift between each pulse pair. In this manner the selective frequency is not at the central spectrometer frequency, but at offset frequencies $(4n+1)\nu$ where $n=0,\pm1,\pm2,...$, and $\nu$ can either be positive or negative depending on the sense of the phase cycling. This is a particularly convenient arrangement since we could perturb a single peak 7000 Hz off resonance and have no other perturbation within 28 000 Hz of our chosen frequency. Typical parameters were a pulse train of 16 pulses of 3.0 $\mu$s, separated by 55 $\mu$s delays with a cyclical phase shift of 90° between successive pulses. This achieved a selective peak inversion. Evolution times were selected to explore mainly the first 200 ms after preparation. The "complementary" experiments consist of preparing a system in which all peaks save one are inverted. This is accomplished by first carrying out the DANTE preparation just described, followed by a composite $\pi$ pulse $[(90)_x-(180)_y-(90)_x]$ utilized because of the 40 kHz sweep width of these experiments.

As in any relaxation experiment, a set of spectra are produced covering the domain of seven or more selected evolution times plus 0 and $\infty$. Block averaging of 16 scans with recovery times of 30 s between scans were used. Typical total scans for the nine or more variable delay times were 1000–10 000 scans, depending on sample, peak intensity, and the desired signal-to-noise ratio in the Bruker spectrometer. On the Varian, we were able to obtain better signal-to-noise ratios with the superior filling factor of a 5 mm probe. Eleven to fifteen variable delays were chosen and typically 512 scans. The $^{129}Xe$ spectrum consists of several peaks attributable to $Xe_1, Xe_2, Xe_3, ..., Xe_8$ clusters. The individual

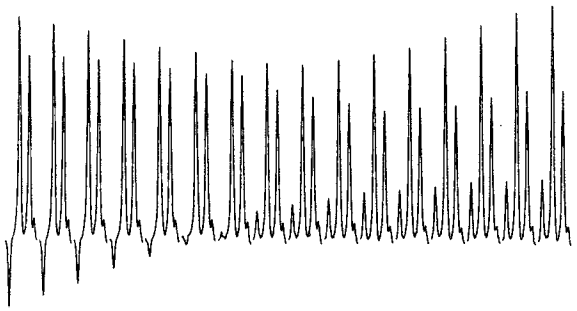

FIG. 2. A typical magnetization experiment. This is a DANTE experiment on $Xe_8$ in a sample with $\langle n\rangle = 6.54$ Xe atoms per alpha cage of zeolite NaA at 300 K. The delay times are (from left to right): 0, 2, 5, 10, 15, 20, 30, 60, 90, 130, 250, 400, 800, 1500, 2500, 3000 ms.

peaks are typically about 9–10 ppm wide. Adjusting the interpulse delays so that the selective region is 9500–11 500 Hz offset from the carrier frequency allows for most of the peak to be inverted. The bandwidth of excitation corresponds to about 600–900 Hz at this offset frequency. Brief exploration at smaller offset frequencies produced excitation bandwidths of as small as 200 Hz which may not be a minimum. There is a clear indication of hole burning, that is, chemical shift dispersion is a major source of the linewidth in this system. Figure 2 is an example of spectra taken at 16 delay times from 0 to 3.0 s.

The 1 K data are zero filled to 4 K, transformed with 300 Hz line broadening, and phase corrected. The substantial first-order phase correction (similar for all spectra) resulted in the necessity of performing a common base-line correction. The transformed spectra were transferred by FASTRAN (T. Farrar, University of Wisconsin). The resulting binary file was converted to an ASCII input for a commercial spectral deconvolution package (GRAMS/386, Galactic Industries). In order to obtain reliable intensities as a function of time, peak position, width, percent Lorentzian/Gaussian were fixed to a common value for each set of 9–16 spectra corresponding to 9–16 delay times that constitute an experiment. In those cases where the inversion was less than 100% efficient, the perturbed peak was fit as the sum of two calculated peaks. The areas from the fitting process, the magnetizations $M(\mathrm{Xe}_n)$, were normalized such that sum of the areas from all the peaks in a given sample at equilibrium equals 1; that is, the normalized $M(\mathrm{Xe}_n)$ at equilibrium is $nf(n)/\langle n\rangle$. Ninety-eight independent magnetization decay/recovery curves were obtained at 300 K for four samples with average occupancies 3.94, 5.80, 6.43, 6.73 Xe atoms per cage on the Bruker spectrometer. The DANTE experiments for the three samples with average loading of 3.94, 5.80, and 6.54 Xe atoms per cage were repeated using the Varian spectrometer.

The analysis of the decay/recovery curves requires the values of the $T_1$ relaxation times for Xe in the zeolite. For these, inversion recovery measurements were carried out on the samples using the Bruker AM-400. For a given sample, a common relaxation rate is observed for all $\mathrm{Xe}_n$ peaks, irrespective of $n$ but the apparent $T_1$ depends on the average number of Xe atoms/cage in the sample. This is consistent with (a) $T_1$ being a function of $n$ and (b) the communication between zeolite cages being sufficiently fast at 300 K to average the relaxation times. At 200 K, different $T_1$ values were observed for each $n$. These relaxation effects will be considered in a later report. For the purpose of our analysis, relaxation rates $R_1(n) = 1/T_1(\mathrm{Xe}_n)$ appear to be 0.1–0.3 $\mathrm{s}^{-1}$, and are much lower than magnetization transfer rates at room temperature. Consequently we used $T_1(\mathrm{Xe}_n)$ of 9.4–3.3 s, varying linearly between $n=1$ and 8. These values are consistent with the distribution-weighted averages which are observed in the inversion recovery experiments and with the long time (beyond 2 s) behavior of the magnetization decay/recovery curves.

## IV. RESULTS

### A. The relations between the phenomenological rate constants and the microscopic rate constants

The phenomenological rate constants $K_{mn}$ in Eq. (2) can be derived in terms of linear combinations of the rate constants $k_{mn}$ for the elementary steps (individual hops from one cage to another). A simple physical picture of the microscopic events which contribute to the overall changes in magnetization that can be observed provides the relationships. One elementary step is shown in Fig. 1 that is characterized by a rate constant $k_{46}$

$$\mathrm{Xe}_6+\mathrm{Xe}_3 \xrightarrow{k_{46}} \mathrm{Xe}_5+\mathrm{Xe}_4$$

in which one Xe atom leaves the $Xe_6$ cluster and jumps into a neighboring cage containing the $Xe_3$ cluster, thereby forming the new cluster $Xe_4$ and the remainder cluster $Xe_5$. Suppose $Xe_6$ is polarized, then the microscopic event pictured in Fig. 1 contributes to the terms $-K_{56}M_6$ and $-K_{46}M_6$ in the $dM_6/dt$ equation, $+K_{56}M_6$ in the $dM_5/dt$ equation, and $+K_{46}M_6$ in the $dM_4/dt$ equation. Suppose $Xe_3$ is polarized. This same microscopic event contributes to the term $+K_{43}M_3$ in the $dM_4/dt$ equation and $-K_{43}M_3$ in the $dM_3/dt$ equation. It can easily be seen that all the microscopic events with rate constants $k_{m_6}$, $m=1,2,3,\ldots,8$ contribute to the $K_{56}M_6$ term in the $dM_6/dt$ and $dM_5/dt$ equations, since one Xe atom jumping out of a cage containing $Xe_6$ always leaves an $Xe_5$ cluster no matter what cage it is jumping into. Similarly, it can be seen that all the microscopic events with rate constants $k_{4n}$, $n=1,2,3,\ldots,8$ contribute to the $K_{43}M_3$ term in the $dM_4/dt$ and $dM_3/dt$ equations since any jump into a cage with $Xe_3$ makes $Xe_4$. On the other hand, *only* this microscopic event illustrated in Fig. 1 with rate constant $k_{46}$ can contribute to the $K_{46}M_6$ term in the $dM_6/dt$ and $dM_4/dt$ equations. From a consideration of the various microscopic events we derive the following relationships:

$$K_{46}=k_{46}f(3) \tag{3}$$

since the probability of finding a $Xe_3$ in a neighboring cage is just $f(3)$ (the fraction of the alpha cages containing $Xe_3$).

$$K_{56}=k_{56}f(4)+5\Sigma_i^8 k_{i6}f(i-1), \tag{4}$$

$$K_{65}=k_{65}f(5)+\Sigma_i^8 i k_{6i}f(i). \tag{5}$$

In general,

$$K_{mn}=k_{mn}f(m-1) \quad \text{provided } |n-m|>1, \tag{6}$$

$$K_{m,m+1}=k_{m,m+1}f(m-1)+m\Sigma_i^8 k_{i,m+1}f(i-1), \tag{7}$$

$$K_{m,m-1}=k_{m,m-1}f(m-1)+\Sigma_i^8 i k_{mi}f(i). \tag{8}$$

Pines *et al.* have derived analogous equations,[8] although their notation is different from ours. However, they used the approximation $K_{m,m+1}=mk_{m,m+1}$ instead of Eq. (7).

We can independently verify the relationships expressed in Eqs. (6)–(8). Given a set of microscopic rate constants $k_{mn}$ in an 8×8 matrix, we derive the values of $K_{mn}$ from the known $f(n)$ of the sample using Eqs. (6)–(8). Then we can solve the simultaneous differential equations (1) by matrix methods for the initial conditions, and plot out the decay/recovery curves. At the same time, we can use the given $k_{mn}$ rate constants in the Monte Carlo simulation to produce the decay and recovery of magnetization for the same initial conditions. Except for statistical errors, the curves should be superimposable for all 138 curves. Indeed we find this to be the case. Therefore, the relations derived between the set of microscopic rate constants $k_{mn}$ and the phenomenological rate constants $K_{mn}$ are correct.

There are constraints on the $K_{mn}$ and the $k_{mn}$ values from principles of detailed balance. For example, it is easily shown that

$$\frac{K_{mn}}{K_{nm}}=\frac{mf(m)}{nf(n)}. \tag{9}$$

It is easily shown that these relations are satisfied by Eqs. (6)–(8). Furthermore, the microscopic rate constants are also subject to the relations

$$\frac{k_{mn}}{k_{nm}}=\frac{mf(m)f(n-1)}{nf(n)f(m-1)} \tag{10}$$

which are merely expressions of the relationships between rate constants and equilibrium constants. The microscopic rate constant for the reverse process of the example in Fig. 1 is $k_{64}$, as in

$$Xe_4+Xe_5 \xrightarrow{k_{64}} Xe_3+Xe_6.$$

From the several relationships generated by Eq. (10) it is possible to deduce the lower triangle of the rate constant matrix $k$ entirely from the initial guess of the upper triangle. No relationship of this type provides information on the diagonal elements $k_{nn}$. One final piece of information: the entire $k$ matrix can be multiplied by a factor without affecting the resulting equilibrium distributions, but the magnetization recovery curves are sensitive to the absolute magnitudes of the $k$ matrix elements, not just their relative magnitudes.

### B. Why not find the phenomenological rate constants directly?

It is possible, in principle, to analyze the recovery curves by using an iterative multiparameter fitting approach, using the algorithms developed by Led *et al.* in their program MTFIT.[13] We did this as well. However, there is an overriding reason why this method would be very difficult to use by itself. One is that the $K$ values that dominate the behavior of the curves are the ones on the band below and above the diagonal of the $K$ matrix since these are made of sums over eight terms. All other $K$ values are much smaller, and these are precisely the ones that have the direct relationship to the microscopic rate constant, that is $K_{68}=k_{68}f(5)$ for example. Under certain conditions, it may be possible to obtain a direct measure of these, but the experimental precision required is very demanding. Furthermore, the phenomenological rate constants are dependent on the sample because the distributions $f(n)$ are different from sample to sample. Therefore, even if we had been able to obtain a complete set of $K$ matrix elements for one sample, this would not have helped us determine the set of phenomenological rate constants for another sample. On the other hand, the microscopic rate constants are independent of sample and depend only on the temperature. One $k$ matrix should reproduce all 138 recovery curves for four samples and also all the equilibrium distributions for all ten samples.

As mentioned above, a measurement of one of the phenomenological rate constants that is directly proportional to the microscopic rate constant would be of great value. With even one such constant one could assign an absolute magnitude to one of the elements in one of the columns of the $k$ matrix which is independent of the values obtained from the overall agreement with experiment that is obtained from the combination of a large number of microscopic rate constants. The experiment involves taking data at very early times when the magnetization change is dominated by just the one $K_{mn}$ for some $|n-m|>1$. Since the value of this phenomenological rate constant is small, the change in the magnetization is also very small. At very early times before any of the other terms in the modified Bloch equation have taken over, the peak intensity versus time will be nearly flat. We did attempt this experiment and we find that even in the most favorable case the small slope in the interval 0–5 ms cannot reliably provide a value of the rate constant. Therefore, the use of simulations to find the set of rate constants for this particular multisite magnetization transfer is the only reasonable approach.

### C. The importance of being at thermal equilibrium

Equation (1) applies to measuring rate constants in a system at equilibrium, and Eqs. (6)–(8) assume that the sample is at the thermal equilibrium mass distribution and that the mass distribution undergoes no net change during the experiment. It should be noted that complete superposition of decay/recovery curves calculated from Eq. (1) using a given $k$ matrix with the magnetization curves resulting from the Monte Carlo simulation using the same $k$ matrix will be obtained only if no net mass transfer is taking place during the magnetization transfer. The simulation keeps track of magnetization changes in $Xe_1$ through $Xe_8$ that are appropriate to whatever net mass transfer is going on among the clusters. In Fig. 3 we show the superposition of the simulated decay/recovery curve with that calculated by solving the differential Eq. (1) using phenomenological rate constants $K$ obtained from Eqs. (6)–(8) with $f(n)$ appropriate to the equilibrium distribution obtained with the rate constant matrix $k$. In contrast, in the bottom of Fig. 3 we show an ex-

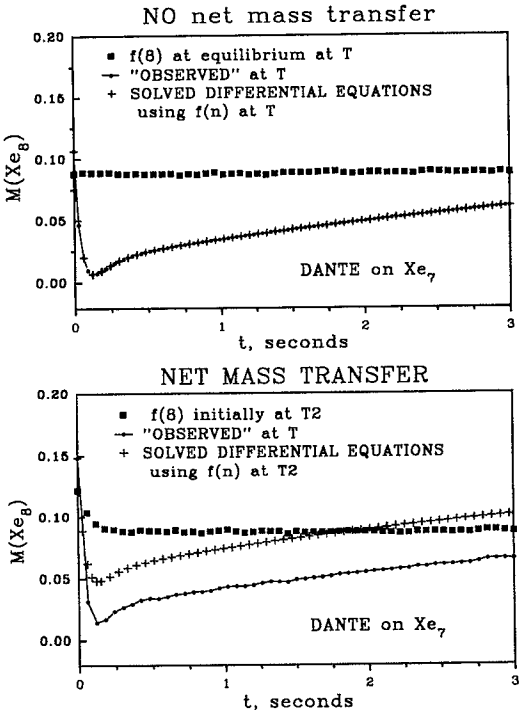


FIG. 3. A comparison of magnetization transfer with and without accompanying mass transfer. The top figure shows a constant $f(8)$, no net mass transfer from one type of cluster to other types. The simulated "observed" magnetization decay/recovery curve (●) is the same as the theoretically expected (+). The bottom figure shows the simulated magnetization curve that would be observed when accompanied by net mass transport (●) is different from that calculated from the magnetization curve that would be observed if the equilibrium mass distribution is the same as the initial mass distribution (+). The changing fraction of cages containing $Xe_n$ at each time step, $f(8)$, is shown (■).

ample in which the initial mass distribution is different from the equilibrium mass distribution toward which the rate constants are driving the system. In the bottom of Fig. 3, the fraction of the 5000 cages that contain $Xe_n$ are shown (■) and the net mass transport accompanying the magnetization recovery can be observed. The drift toward the equilibrium mass distribution appropriate to the rate constants, away from the initial mass distribution, accompanies the recovery of magnetization and distorts the decay/recovery curve. This could happen if the initial mass distribution is appropriate to a higher or lower temperature than the temperature at which the magnetization transfer experiments are being carried out. For the given $k$ matrix, the simulated curve (●) is what would be observed. The calculated curves (+) are those obtained from solving Eq. (1) using the same $k$ matrix and the equilibrium $f(n)$ at temperature $T2$, that is, the curve that would have been observed if the magnetization transfer experiments had been carried out at the temperature $T2$ of the mass distribution. Obviously, the rate constants that would have been obtained from the lower figure curve (●) are not the same as the rate constants that would have been obtained from the curve (+) nor are they the same as would have been obtained from both (●) and (+) in the upper figure, where the magnetization transfer and the equilibrium mass distribution are for the same temperature $T$. The conclusion from Fig. 3 is that it is important to carry out the magnetization transfer experiment with a sample that is at the equilibrium mass distribution for the temperature of the experiment. Otherwise, inaccurate rate constants (which include the effects of net mass transport) may be obtained. A variable temperature study must therefore use samples that are at their equilibrium mass distribution at each temperature. On the other hand, this particular simulation presents an extreme case. In actual nonequilibrium experiments, there are concentration gradients (not simulated here) which exist on a macroscopic scale. These gradients prevent the system from responding on a time scale as short as this simulation exhibits. In the simulation each cage is treated as being equally probable in communicating with all the other 4999 cages, rather than there existing local, nearly steady-state dynamics such that the system approaches equilibrium on a time scale of days, as actually found in our sample preparation.

### D. The rate constants that drive the hypergeometric distribution

The limiting situation offered by the strictly statistical distribution (the hypergeometric distribution) may provide some insight. We have already seen[5,6] that the experimental equilibrium distributions, especially at high loading, do not agree with a hypergeometric distribution. Nevertheless, the statistical distribution provides a limiting case against which we can compare the actual data. We have seen in Eq. (10) that detailed balance determines the ratios of the conjugate rate constants, $k_{mn}/k_{nm}$. Since the hypergeometric distribution provides an analytical expression for the $f(n)$, then the ratios $k_{mn}/k_{nm}$ that are compatible with the hypergeometric distribution can be derived from Eq. (10). These ratios are as follows, the ratios shown are $k_{(\text{row,col})}/k_{(\text{col,row})}$:

| | 1 | 2 | 3 | 4 | 5 | 6 | 7 |
|---|---|---|---|---|---|---|---|
| 2 | 7/8 | | | | | | |
| 3 | 6/8 | 6/7 | | | | | |
| 4 | 5/8 | 5/7 | 5/6 | | | | |
| 5 | 4/8 | 4/7 | 4/6 | 4/5 | | | |
| 6 | 3/8 | 3/7 | 3/6 | 3/5 | 3/4 | | |
| 7 | 2/8 | 2/7 | 2/6 | 2/5 | 2/4 | 2/3 | |
| 8 | 1/8 | 1/7 | 1/6 | 1/5 | 1/4 | 1/3 | 1/2 |

An interesting characteristic of these ratios is that they systematically decrease in going down each column and left to right across each row. The discrepancy between the rate constants for the forward and back elementary steps becomes more pronounced with increasing difference in the cluster sizes in the "from" and "to" cages.

Using the hypergeometric distribution constraint on the ratios of the microscopic rate constants, and assuming $k_{88}=k_{78}=\cdots=k_{18}=1$, we find that we can generate the entire matrix of rate constants that are consistent with this statistical distribution. A $k$ matrix consistent with the hypergeometric distribution is as follows:

| Leaving / Forming | 1 | 2 | 3 | 4 | 5 | 6 | 7 | 8 |
|---|---|---|---|---|---|---|---|---|
| 1 | 1/8 | 1/7 | 1/6 | 1/5 | 1/4 | 1/3 | 1/2 | 1 |
| 2 | 1/8 | 1/7 | 1/6 | 1/5 | 1/4 | 1/3 | 1/2 | 1 |
| 3 | 1/8 | 1/7 | 1/6 | 1/5 | 1/4 | 1/3 | 1/2 | 1 |
| 4 | 1/8 | 1/7 | 1/6 | 1/5 | 1/4 | 1/3 | 1/2 | 1 |
| 5 | 1/8 | 1/7 | 1/6 | 1/5 | 1/4 | 1/3 | 1/2 | 1 |
| 6 | 1/8 | 1/7 | 1/6 | 1/5 | 1/4 | 1/3 | 1/2 | 1 |
| 7 | 1/8 | 1/7 | 1/6 | 1/5 | 1/4 | 1/3 | 1/2 | 1 |
| 8 | 1/8 | 1/7 | 1/6 | 1/5 | 1/4 | 1/3 | 1/2 | 1 |

We find then, that the strictly statistical hypergeometric distribution is consistent with all elements in a column being the same. This is true for all columns and means that the rate of leaving a cage depends only on the occupancy of the departure cage and not the occupancy of the destination cage. It should be noted that, to produce the strictly statistical hypergeometric distribution, the rate constant for a single Xe atom leaving a cage containing $Xe_n$ increases with increasing $n$.

Of course, these are only relative values; the whole $k$ matrix can be multiplied by an arbitrary factor and the resulting equilibrium distribution would still be the hypergeometric distribution. We verified that when the above $k$ matrix is used in the simulation program for samples ranging from $\langle n\rangle = 0.45$ to 6.73 the simulations arrived at the hypergeometric distributions appropriate to the value of $\langle n\rangle$ in each case. The experimental distributions at room temperature are significantly different from the hypergeometric distribution for the five samples with $\langle n\rangle$ greater than 4.0. The rate constants that produce the hypergeometric distribution cannot reproduce the experimental magnetization decay/recovery curves. The multiplicative factor can be adjusted so as to reproduce selected curves, but the predicted curves for all other experiments then bear little similarity to the experimental ones. Some examples are shown in Fig. 4. Since we have 138 curves to compare with, it is easily proven that the above rate constants are not correct. Nevertheless, it is instructive to see this limiting case because the experimental $k$ matrix should differ from this one in ways that can be projected by physical insight. If indeed, the distribution at very high temperatures (523 K, for example) are nearly the same as the hypergeometric distribution,[14] then at room temperature the ratio of $k$ matrix elements $k_{m2}/k_{m1}$ would probably be less than predicted by the hypergeometric distribution, because of the attractive interaction between the two Xe atoms that is not present for a single Xe atom in a cage. We expect, by the same reasoning, that the difference between $k_{m3}$, $k_{m4}$,..., or $k_{m8}$ and $k_{m1}$ would be more pronounced than hypergeometric. If this is the case, then, from the "hypergeometric" rate constants above, we might expect to find that $k_{m4}/k_{m1}<8/5$, $k_{m3}/k_{m1}<8/6$, $k_{m2}/k_{m1}<8/7$, and also $k_{m8}/k_{m1}<8$, $k_{m7}/k_{m1}<4$, and $k_{m6}/k_{m1}<8/3$. Of course, it is the differing energies of activation for each of the $k_{m1}, k_{m2},\ldots,k_{m8}$ that make such distinctions. In the limit of very high temperatures, the rate constants might well relate to each other in the hypergeometric sense.

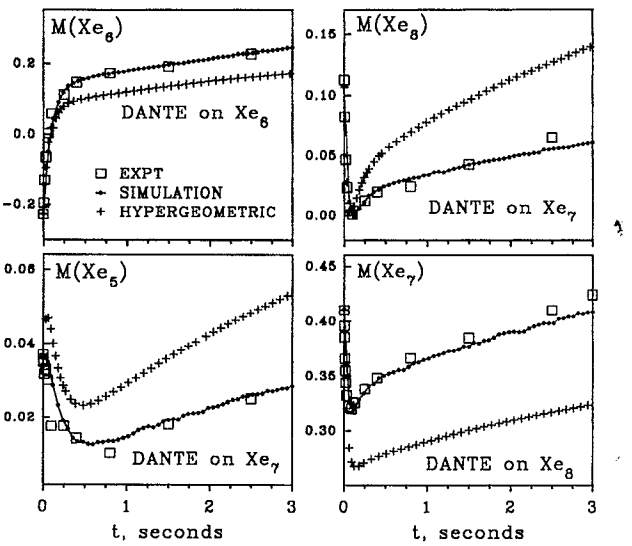


FIG. 4. The rate constant matrix that drives the hypergeometric distribution (see the text) leads to magnetization recovery curves that are drastically different from experiment.

## E. The microscopic rate constants

Next we need to know whether or not we can find a set of microscopic rate constants capable of reproducing the 138 experimental recovery curves obtained from four samples and also the experimental equilibrium values of $f(n)$ for all ten samples. To start with, we make the simple assumption that the probability of a Xe atom leaving a cluster $Xe_n$ depends only on the nature of $Xe_n$ and not on the occupancy of the cage it will jump into, that is $k_{1n}=k_{2n}=k_{3n}=\cdots=k_{8n}$. This is a reasonable assumption for small $m$ certainly, because the entryway into the cage containing $Xe_{m-1}$ for $m-1=0$ to 4 probably looks the same to the Xe atom attempting to cross over. On the other hand if the receiving cage is overcrowded, containing six or seven atoms, or even eight atoms, there is a significant probability that the the entryway may be blocked during the jump. Therefore, we might expect that the simple assumption that the rate of leaving a cage with $Xe_n$ is independent of the occupancy of the destination cage may not be valid for large $m$, since indeed we are assuming the rate goes to zero for $m=9$.

The ratios of the rate constants can be obtained from experiment directly. As seen in Eq. (10) each ratio $k_{mn}/k_{nm}$ is usually determined by four values of $f(n)$. Those samples that have large enough values of $f(n)$, $f(m)$, $f(n-1)$, $f(m-1)$ will provide reliable ratios. Therefore it is possible to arrive at some set of $k$ ratios that are consistent with experimental distribution of occupancies, but certainly not possible to determine all such ratios. Since many samples have some $f(n)$ values that are too small to be reliable we have incomplete information. The hypergeometric values however exhibit the same trends in the $k$ ratios going down and to the right of the array. This allows us to make estimates of those ratios that are not experimentally known. We started out with the premise that the $k_{mn}$ are the same for a given $n$, assumed a value of $k_{m1}$, then used the $k$ ratios to determine the next

TABLE I. The microscopic rate constants ($s^{-1}$) used in the simulations. The notation used is that $k_{mn}$ is the rate constant for the event in which a single Xe atom leaves the cage containing the cluster $Xe_n$ jumping into the neighboring cage to form cluster $Xe_m$, $Xe_n + Xe_{m-1} \xrightarrow{k_{mn}} Xe_{n-1} + Xe_m$.

| | Leaving | | | | | | | |
|---|---|---|---|---|---|---|---|---|
| Forming | 1 | 2 | 3 | 4 | 5 | 6 | 7 | 8 |
| 1 | 0.300 | 0.320 | 0.325 | 0.322 | 0.477 | 0.892 | 1.20 | 2.50 |
| 2 | 0.351 | 0.320 | 0.325 | 0.322 | 0.477 | 0.892 | 1.20 | 2.50 |
| 3 | 0.355 | 0.360 | 0.325 | 0.322 | 0.477 | 0.892 | 1.29 | 2.50 |
| 4 | 0.289 | 0.364 | 0.319 | 0.322 | 0.477 | 0.892 | 1.20 | 2.50 |
| 5 | (0.286) | 0.381 | 0.334 | 0.322 | 0.477 | 0.892 | 1.20 | 2.50 |
| 6 | (0.268) | 0.357 | 0.341 | 0.322 | 0.477 | 0.892 | 1.20 | 2.50 |
| 7 | (0.108) | (0.120) | 0.118 | 0.144 | 0.147 | 0.277 | 1.20 | 2.50 |
| 8 | (0.100) | (0.115) | (0.115) | (0.115) | 0.191 | 0.095 | 0.456 | 2.50 |

column of numbers. This process can be propagated from one column to the next, sequentially. This provided a first guess for a $k$ matrix for the simulations. The final $k$ matrix of microscopic rate constants that we used in the simulations to compare with experiment is given in Table I. In Figs. 5–7 we show a few of the 138 decay/recovery curves obtained by simulation using the assumed $k$ matrix (●), by solution of

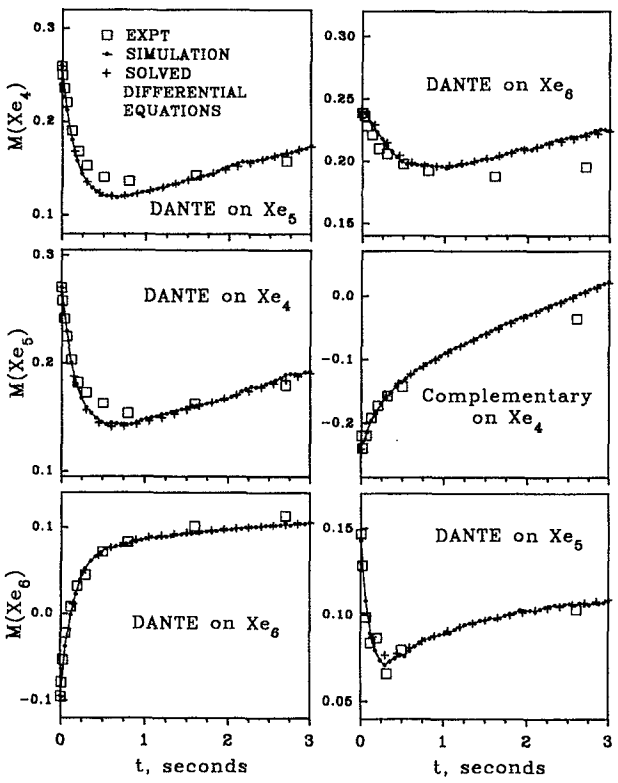


FIG. 5. The simulations using the rate constant matrix in Table I shown as (●) connected by straight lines, are compared with the magnetization recovery curves calculated from the phenomenological rate constants $K$ which are derived from the matrix $k$ in Table I by Eqs. (6)–(8) (+), and with the experimental data points (□). These curves are some of the magnetization decay/recovery curves for $Xe_4$, $Xe_5$, and $Xe_6$ in the sample with $\langle n \rangle = 3.94$ at 300 K. The type of experiment and the perturbed peak label each subfigure.

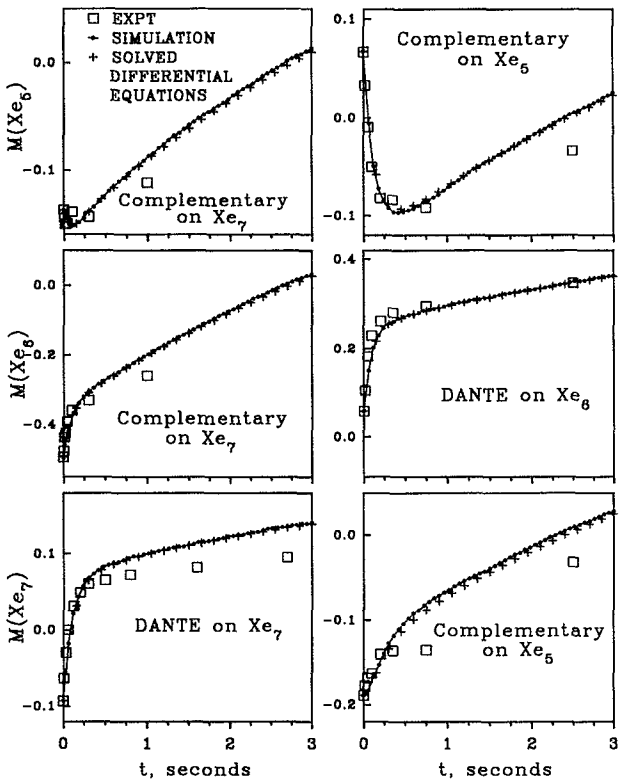


FIG. 6. The same symbols as in Fig. 5. These curves are some of the magnetization decay/recovery curves for $Xe_5$, $Xe_6$, and $Xe_7$ in the sample with $\langle n \rangle = 5.80$ at 300 K.

Eq. (1) with the $K$ values derived from this $k$ matrix (+), and from the experimental data (□). In each case we have verified the lack of net mass transport; the fraction of the 5000 cages that contain $n$ Xe atoms at each time step is plotted (not shown here) and this shows no systematic drift.

These figures (5–7) were selected to indicate the variety of curves which we have observed. Curves for DANTE and complementary experiments were obtained in the Bruker AM-400 spectrometer for four samples (98 curves) and DANTE experiments for three samples (40 curves) in the Varian VXR-300S. Most of the curves from the complementary experiments are purely recovery curves and for these the experiments and simulations are near coincident. Only a few of those are shown here. The more demanding comparisons are for the curves which are decay followed by recovery, exhibiting a bowl, typical of the curves from the DANTE experiments. The important thing to note is that where there might appear to be a systematic deviation between the simulation and the experiment in the figures, this is not really the case. For each curve observed in both spectrometers, the simulation is bracketed by the two sets of experimental points. In other words, the agreement between experiment and simulation is within the combined random and systematic experimental errors.

As further evidence we present in Fig. 8 the equilibrium $f(n)$ values reached by simulations using the $k$ matrix given in Table I, in comparison with the experimental equilibrium distributions for the ten samples. We find that the $k$ matrix given in Table I which reproduces the 138 decay/recovery

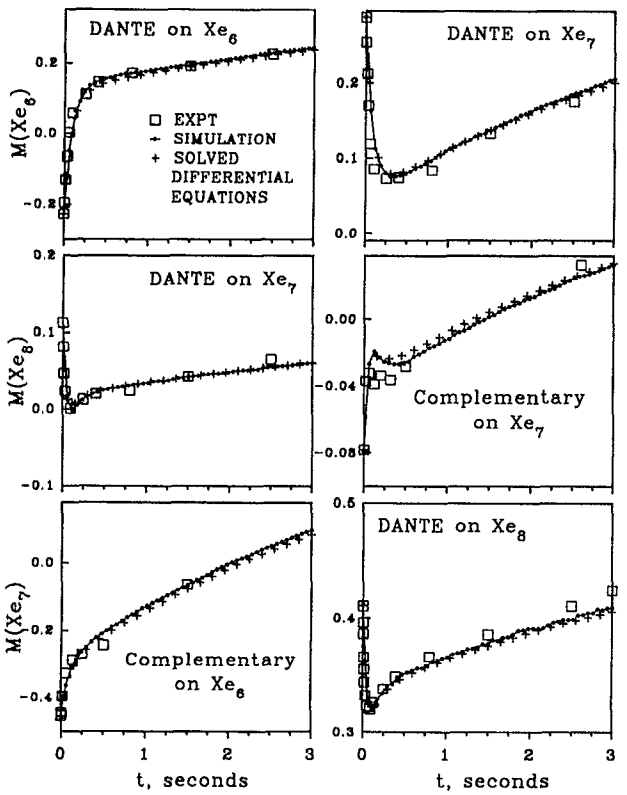


FIG. 7. The same symbols as in Fig. 5. These curves are some of the magnetization decay/recovery curves for $Xe_6$, $Xe_7$, and $Xe_8$ in the sample with $\langle n \rangle = 6.54$ at 300 K.

curves for four samples at 300 K also reproduces the equilibrium distributions of all ten samples. The deviations from the equilibrium $f(n)$ are all less than 0.03; the overall standard deviation is $8.3 \times 10^{-3}$. The agreement with experiment is within experimental error.

In examining the $k$ matrix in Table I we note several important characteristics. The rate constant associated with a single Xe atom leaving a particular $Xe_n$ is relatively independent of the destination, the elements in each column being fairly similar. This is not true when the destination cage is already highly populated. We note this in $k_{73}$, $k_{74}$, $k_{75}$, and $k_{76}$ and in $k_{85}$, $k_{86}$, and $k_{87}$. These rate constants are much smaller than the others in the same column and the experimental results are sensitive to them. Other rate constants such as $k_{71}$, $k_{72}$, $k_{81}$, $k_{82}$, $k_{83}$, and $k_{84}$ are also made smaller by our assumed $k$ ratio, but the experiments are not sensitive to these because we have no samples containing observable peaks for both $Xe_8$ and $Xe_1$, etc. In Table I, these rate constants which are not tested directly by experiments are enclosed in parentheses. These are used in the simulation but only affect the details in the approach to the equilibrium distribution (which is not observed experimentally). It is difficult to place error bars on the rate constants in Table I because we have not conducted a complete sensitivity analysis. Some of the relationships among these numbers are quite precisely known and well tested. Therefore the relative magnitudes are quite precise in some cases. On the other hand, the absolute magnitudes of each one by itself is not nearly as precisely bracketed by the experiments. Perhaps 20%–30% error in the individual absolute magnitude would be a conservative estimate. At the same time the absolute magnitude of sums of terms that are represented by the large phenomenological rate constants are also fairly well bracketed by the

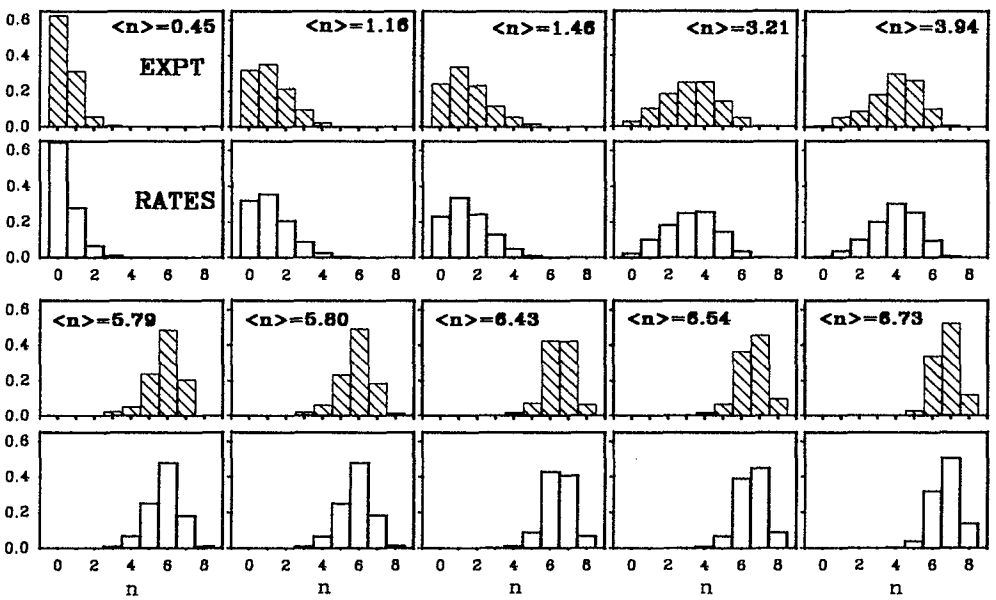


FIG. 8. The simulated equilibrium distributions resulting from the rate constant matrix in Table I, for ten samples starting from a uniform distribution at time zero. The experimental distributions are shown for comparison.

TABLE II. Phenomenological rate constants for three samples, calculated using Eqs. (6)–(8) and the $f(n)$ at the simulated equilibrium. $K_{ii}$ (not given here) is related to the off-diagonal values by Eq. (2).

| $f(n)$ | $\langle n\rangle$=3.938 | | | | | | | |
|---|---|---|---|---|---|---|---|---|
| 0.005 44 | 0.036 51 | 0.099 16 | 0.199 09 | 0.303 66 | 0.253 65 | 0.094 68 | 0.007 57 | 0.000 24 |
| | 1 | 2 | 3 | 4 | 5 | 6 | 7 | 8 |
| 1 | | 0.341 84 | 0.001 77 | 0.001 75 | 0.002 59 | 0.004 85 | 0.006 53 | 0.013 60 |
| 2 | 1.854 42 | | 0.630 000 | 0.011 76 | 0.017 42 | 0.032 57 | 0.043 81 | 0.091 27 |
| 3 | 0.035 16 | 1.885 37 | | 0.942 84 | 0.047 30 | 0.088 45 | 0.118 99 | 0.247 90 |
| 4 | 0.057 57 | 0.072 44 | 1.907 56 | | 1.869 13 | 0.177 59 | 0.238 91 | 0.497 72 |
| 5 | 0.086 91 | 0.115 79 | 0.101 33 | 1.954 67 | | 4.408 72 | 0.364 39 | 0.759 15 |
| 6 | 0.067 88 | 0.090 50 | 0.086 45 | 0.081 75 | 1.976 82 | | 7.468 85 | 0.634 12 |
| 7 | 0.010 23 | 0.011 36 | 0.011 13 | 0.013 63 | 0.013 95 | 0.712 04 | | 17.732 00 |
| 8 | 0.000 76 | 0.000 87 | 0.000 87 | 0.000 87 | 0.001 44 | 0.000 72 | 0.563 11 | |
| $f(n)$ | $\langle n\rangle$=5.80 | | | | | | | |
| 0.000 01 | 0.000 07 | 0.001 04 | 0.009 74 | 0.064 03 | 0.249 14 | 0.478 55 | 0.183 86 | 0.013 56 |
| | 1 | 2 | 3 | 4 | 5 | 6 | 7 | 8 |
| 1 | | 0.195 83 | 0.000 00 | 0.000 00 | 0.000 00 | 0.000 01 | 0.000 01 | 0.000 03 |
| 2 | 5.063 70 | | 0.374 36 | 0.000 02 | 0.000 03 | 0.000 06 | 0.000 08 | 0.000 17 |
| 3 | 0.000 37 | 5.064 14 | | 0.583 76 | 0.000 50 | 0.000 93 | 0.001 25 | 0.002 60 |
| 4 | 0.002 82 | 0.003 54 | 5.066 68 | | 1.045 39 | 0.008 69 | 0.011 69 | 0.024 35 |
| 5 | 0.018 33 | 0.024 42 | 0.021 37 | 5.084 74 | | 2.253 49 | 0.076 84 | 0.160 08 |
| 6 | 0.066 67 | 0.088 89 | 0.084 91 | 0.080 29 | 5.183 38 | | 6.580 31 | 0.622 85 |
| 7 | 0.051 68 | 0.057 43 | 0.056 28 | 0.068 91 | 0.070 52 | 2.969 15 | | 18.459 07 |
| 8 | 0.018 39 | 0.021 14 | 0.021 14 | 0.021 14 | 0.035 07 | 0.017 47 | 1.485 00 | |
| $f(n)$ | $\langle n\rangle$=6.543 | | | | | | | |
| 0.000 00 | 0.000 00 | 0.000 02 | 0.000 50 | 0.007 69 | 0.065 70 | 0.390 56 | 0.448 42 | 0.087 12 |
| | 1 | 2 | 3 | 4 | 5 | 6 | 7 | 8 |
| 1 | | 0.125 00 | 0.000 00 | 0.000 00 | 0.000 00 | 0.000 00 | 0.000 00 | 0.000 00 |
| 2 | 7.766 50 | | 0.245 25 | 0.000 00 | 0.000 00 | 0.000 00 | 0.000 00 | 0.000 00 |
| 3 | 0.000 01 | 7.766 51 | | 0.394 89 | 0.000 01 | 0.000 02 | 0.000 02 | 0.000 05 |
| 4 | 0.000 14 | 0.000 18 | 7.766 66 | | 0.713 65 | 0.000 45 | 0.000 60 | 0.001 25 |
| 5 | 0.002 20 | 0.002 93 | 0.002 57 | 7.769 00 | | 1.091 29 | 0.009 23 | 0.019 22 |
| 6 | 0.017 58 | 0.023 44 | 0.022 39 | 0.021 17 | 7.797 98 | | 4.649 23 | 0.164 25 |
| 7 | 0.042 18 | 0.046 87 | 0.045 93 | 0.056 24 | 0.057 55 | 6.320 65 | | 16.951 98 |
| 8 | 0.044 84 | 0.051 57 | 0.051 57 | 0.051 57 | 0.085 54 | 0.042 60 | 3.666 33 | |

overall shapes of the multitude of the decay/recovery curves.

The $k$ matrix in Table I can be compared with the $k$ matrix reported by Pines *et al.*[8] At the outset they had assumed $k_{mn}$ to be independent of $m$ and their values obtained from two-dimensional spectra at room temperature [from their Fig. 3(a)] are: $k_{m1}=0.09$, $k_{m2}=0.08\pm0.02$, $k_{m3}=0.05$, $k_{m4}=0.06\pm0.02$, $k_{m5}=0.11\pm0.07$, $k_{m6}=0.26\pm0.10$, $k_{m7}=0.82\pm0.15$ $s^{-1}$. These are of the same order of magnitude as the rate constants we have arrived at, but our values are systematically larger than theirs, in most cases by a factor of 3–5. They assumed identical intrinsic rate constants regardless of the number of Xe atoms in the destination cage. We have found it impossible to fit our experimental distributions without using smaller rate constants when the number of Xe atoms in the destination cage is six or seven prior to migration. On the other hand, Pines *et al.* have done their two-dimensional experiments at 336 and 357 K as well, and have reported the free energy differences from their variable temperature work and also estimates of the activation energies.

The $K$ matrix for three of the samples that we used are shown in Table II in order to illustrate the changes of the phenomenological rate constants with sample and their relative magnitudes within each sample. We have also examined the relative contributions of the various terms to each of the one-off-the-diagonal $K_{mn}$ (the ones that are composed of eight terms). In every case, there are at least two, more often three to four, of the eight terms that are comparable in magnitude. This was true for all four samples, which clearly demonstrates that none of these $K_{mn}$ can be considered to be dominated by a single term. This negates the possibility of making a simplifying assumption that a single term dominates the one-off-the-diagonal phenomenological rate constants.

In the interpretation of the magnetization transfer experiments, we have considered only a particular fundamental event, that of a single Xe atom leaving one cage and entering a second cage. With the Na(II) ions blocking the windows of the alpha cage it is not necessary to consider two Xe atoms going through the same window at the same time. If such were significant one would expect the time evolution curves involving $K_{i,i+2}$ and $K_{i,i-2}$ to possess a contribution from a single exponential. We did not observe any evidence of a two-atom transfer in a correlated manner. However, a more

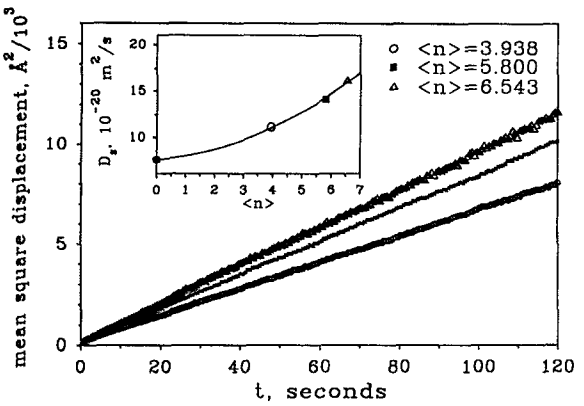


FIG. 9. The results of the simulation of the diffusion of Xe in the cages of zeolite NaA, using the rate constant matrix given in Table I.

plausible correlated event involving two Xe atoms could be involved in crowded cages: one Xe atom coming in through one window of the cage pushes another one out of the opposite (or other) window. In this case, instead of $K_{84}$ being equal to $k_{84}f(7)$ we should add also $k_{84}f(8)$, for example, since the "transit" cage preserves its occupancy number. We have no evidence of this type of correlated two-atom event.

### F. The diffusion rate of Xe atoms in zeolite NaA

With the elementary rate constant matrix at 300 K which provide a good simulation of the magnetization transfer experiments and also reproduce the equilibrium distributions at 300 K, we can simulate the self-diffusion of Xe atoms in zeolite NaA, using a similar procedure. For this purpose only the coordinates of the cage are considered, not the position of the Xe atom within the alpha cage. Ten by ten by ten alpha cages form the simulation box. Periodic boundary conditions are used, that is, if a Xe atom finds itself in an alpha cage outside of the simulation box, the image of the present configuration of the simulation box is used to provide the cage occupancy. As before, a uniform distribution is the preliminary state, 100 equilibration steps are taken in which each Xe atom is allowed a choice of six windows $(+x,-x,+y,-y,+z,-z)$ and to attempt a random jump with a probability according to the value of the microscopic rate constant appropriate to the occupancy of the cage in which it finds itself and the cage it is attempting to jump into. The equilibrium distribution arrived at in this simulation is the same as was found with the simulation using 5000 cages without regard to spatial location. After the equilibration steps, the simulation of the diffusion begins. The zero time coordinates of each Xe atom is recorded and its mean square distance from its initial coordinates is recorded every five time steps. The simulation is allowed to proceed for 120 s. Figure 9 shows the mean square displacement $x^2+y^2+z^2$ (averaged over all atoms, 3938 up to 6543 Xe atoms, according to the average loading for the sample) for three samples of Xe in zeolite NaA. The diffusion coefficient (the self-diffusivity, $D_s$) obtained from the slope by using Einstein's diffusion equation

$$D_s=\left(\frac{1}{6}\right)\lim_{t\to\infty}\frac{d}{dt}\langle|\mathbf{r}(t)-\mathbf{r}(0)|^2\rangle$$

is 0.073 (cage length)$^2$ per second or $0.11\times10^{-18}$ m$^2$/s for the sample with $\langle n\rangle=3.938$ Xe atoms per cage, 0.092 (cage length)$^2$ per second or $0.14\times10^{-18}$ m$^2$/s for the sample with $\langle n\rangle=5.80$ Xe atoms per cage, and 0.10 (cage length)$^2$ per second or $0.16\times10^{-18}$ m$^2$/s for the sample with $\langle n\rangle=6.543$ Xe atoms per cage. The self-diffusivity at the zero-loading limit, $D_s=0.075\times10^{-18}$ m$^2$/s was obtained in exactly the same way as all the others, except that the rate constant $k_{11}$ was used in every attempt to jump. Since the mean square displacement is equal to the number of steps for a random walk on a simple cubic lattice, and the rate constant is just the number of steps per unit time, $D_s=k/6$ in units of (cage length)$^2$/s. Using the rate constant $k_{11}$ for the zero-loading limit, and using the average rate constant for a given $\langle n\rangle$ is

$$\langle k\rangle=\Sigma_{n=1}^{8}\Sigma_{m=1}^{8}f(m-1)k_{mn}f(n)$$

leads to values of $D_s$ equal to 0.075, 0.10, 0.13, and $0.16\times10^{-18}$ m$^2$/s for $\langle n\rangle=0.0$, 3.94, 5.80, and 6.54, respectively, which agree with the results of the simulations. The larger diffusion rate for the higher loading is a reflection of the intrinsically higher probability of a single Xe atom making a jump out of a cage containing $Xe_n$ being higher for larger $n$. This is in contrast to the self-diffusivity of Xe monotonically decreasing with increasing concentration in silicalite, found experimentally[15] and also predicted by equilibrium molecular dynamics simulations.[16] It is also in contrast to the self-diffusivity of methane monotonically decreasing with increasing concentration in silicate observed experimentally[17,18] and predicted by equilibrium molecular dynamics simulations.[16,19,20] This is a very slow diffusion rate when compared to those measured for Xe self-diffusion in the more open zeolites such as NaCaA, NaX, or silicalite, in which $D_s$ is of the order of $10^{-8}$ m$^2$/s.[21] These diffusion coefficients are also smaller than those estimated for methane in zeolite NaA: $D_s=10^{-15}$ m$^2$/s by adsorption techniques,[22] or $5\times10^{-16}$ or $3.8\times10^{-15}$ m$^2$/s,[4] estimated from mean cage residence times deduced from measurements of NMR spin relaxation times ($T_2$). The monotonic increase of the self-diffusivity with concentration shown in the inset in Fig. 9, is classified by Kaerger and Pfeifer[23] as type V behavior, typical of cases in which the critical diameters of the intracrystalline pore system are of the order of the molecular diameters, as for propane at 413 K in zeolite NaCaA.[24]

## V. CONCLUSIONS

We have determined the rate constants $k_{mn}$ for the individual cage-to-cage transfer of a single Xe atom from a cage containing a cluster $Xe_n$ to a cage containing a cluster $Xe_{m-1}$ to form $Xe_m$ at 300 K. In general the rate constant for a single Xe atom leaving a cage increases with increasing occupancy. These rate constants are nearly independent of the occupancy of the recipient cage except in the cases where this occupancy is 6, 7, or 8. The rate constants decrease dramatically for a Xe atom jumping into a cage containing $Xe_6$, $Xe_7$, or $Xe_8$. Since we have observed no $Xe_9$ at all, the ratio $k_{9m}/k_{m9}$ must be very small, that is, $k_{9m}$ is very small

and/or $k_{m9}$ is very large. We find that the rate constant matrix which reproduces the very large number of experimental magnetization decay/recovery curves also leads to an equilibrium distribution of Xe atoms among the cages that is in very good agreement with experiment for all ten samples. What remains to be done is the application of transition state theory to the a priori calculation of the rate constants obtained here.

## ACKNOWLEDGMENTS

This research has been supported by the National Science Foundation (Grant No. CHE92-10790). Some of the results reported here have been presented at the Symposium on Molecules in Restricted Geometries, ACS National Meeting in Denver, March 1993. C.J.J. is grateful to Professor John Rowlinson for his hospitality during C.J.J.'s visit to Oxford University, during which time the simulations presented here were initiated, inspired by a suggestion offered by him.

[1] E. Cohen de Lara, R. Kahn, and F. Mezei, J. Chem. Soc., Faraday Trans. 1 **79**, 1911 (1983).
[2] J. Kaerger and D. M. Ruthven, Zeolites **9**, 267 (1989).
[3] E. Cohen de Lara and R. Kahn, Zeolites **12**, 256 (1992).
[4] J. M. Alloneau and F. Volino, Zeolites **6**, 431 (1986); D. Freude, *ibid.* **6**, 12 (1986).
[5] C. J. Jameson, A. K. Jameson, R. Gerald II, and A. C. de Dios, J. Chem. Phys. **96**, 1676 (1992)
[6] C. J. Jameson, A. K. Jameson, B. I. Baello, and H. M. Lim, J. Chem. Phys. **100**, 5965 (1994).
[7] A. K. Jameson, C. J. Jameson, and R. E. Gerald II, presented at the American Chemical Society National Meeting, Denver, CO, March 1993 (unpublished)
[8] A. Pines, in Ref. 7; R. G. Larsen, J. Shore, K. Schmidt-Rohr, L. Emsley, H. Long, A. Pines, M. Janicke, and B. F. Chmelka, Chem. Phys. Lett. **214**, 220 (1993).
[9] G. A. Morris and R. Freeman, J. Magn. Reson. **29**, 433 (1978).
[10] H. Gesmar and J. J. Led, J. Magn. Reson. **68**, 95 (1986).
[11] D. R. Muhandiram and R. E. D. McClung, J. Magn. Reson. **71**, 187 (1987).
[12] J. J. Led and H. Gesmar, J. Magn. Reson. **49**, 444 (1982).
[13] MTFIT, Jens Led, Department of Chemical Physics, University of Copenhagen, The Oersted Institute, 5 Universitetsparken, DK-2100 Copenhagen Ø, Denmark.
[14] B. F. Chmelka, D. Raftery, A. V. McCormick, L. C. de Menorval, R. D. Levine, and A. Pines, Phys. Rev. Lett. **66**, 580 (1991); **67**, 931 (1991)
[15] W. Heink, J. Kaerger, H. Pfeifer, and F. Stallmach, J. Am. Chem. Soc. **112**, 2175 (1990).
[16] R. L. June, A. T. Bell, and D. N. Theodorou, J. Phys. Chem. **94**, 8232 (1990).
[17] H. Jobic, M. Bee, J. Caro, M. Beulow, and J. Kaerger, J. Chem. Soc. Faraday Trans. 1 **85**, 4201 (1989).
[18] J. Caro, M. Beulow, W. Schirmer, J. Kaerger, W. Heink, H. Pfeifer, and S. P. Zhdanov, J. Chem. Soc. Faraday Trans. 1 **81**, 2541 (1985).
[19] E. J. Maginn, A. T. Bell, and D. N. Theodorou, J. Phys. Chem. **97**, 4173 (1993).
[20] J. R. Hufton, J. Phys. Chem. **95**, 8836 (1991).
[21] J. Kaerger, H. Pfeifer, F. Stallmach, N. N. Feoktistova, and S. P. Zhdanov, Zeolites **13**, 50 (1993).
[22] D. M. Ruthven and R. Kumar, Can. J. Chem. Eng. **57**, 342 (1979).
[23] J. Kaerger and H. Pfeifer, Zeolites **7**, 90 (1987).
[24] J. Kaerger and D. M. Ruthven, J. Chem. Soc. Faraday Trans. 1 **77**, 1485 (1981).